

Histogram of Gradient Orientations of Signal Plots applied to P300 Detection

Rodrigo Ramele^{1,*}, Ana Julia Villar¹ and Juan Miguel Santos¹

¹*Centro de Inteligencia Computacional, Computer Engineering Department,
Instituto Tecnológico de Buenos Aires, Buenos Aires, Argentina*

Correspondence*:

Rodrigo Ramele, C1437FBH Lavarden 315, Ciudad Autónoma de Buenos Aires,
Argentina
rramele@itba.edu.ar

2 ABSTRACT

3 Word Count: 4841

4 The analysis of Electroencephalographic (EEG) signals is of ulterior importance for decoding
5 patterns that could improve the implementation of Brain Computer Interfaces (BCI). These
6 systems are meant to provide alternative pathways to transmit volitional information which could
7 potentially enhance the quality of life of patients affected by neurodegenerative disorders and
8 other mental illness. Of particular interests are those which are based on the recognition of
9 Event-Related Potentials (ERP) because they can be elicited by external stimuli and used to
10 implement spellers, to control external devices or even avatars in virtual reality environments.
11 This work mimics what electroencephalographers have been doing clinically, visually inspecting
12 and categorizing phenomena within the EEG by the extraction of features from images of signal
13 plots. It also aims to provide a framework to analyze, characterize and classify EEG signals, with
14 a focus on the P300, an ERP elicited by the oddball paradigm of rare events. The validity of the
15 method is shown by offline processing a public dataset of Amyotrophic Lateral Sclerosis (ALS)
16 patients and an own dataset of healthy subjects.

17 **Keywords:** electroencephalography, histogram of gradient orientations, brain-computer interfaces, P300, SIFT, amyotrophic lateral
18 sclerosis, naive-bayes near neighbours, waveforms 

1 INTRODUCTION

19 Although recent advances in neuroimaging techniques, particularly radio-nuclear and radiological
20 scanning methods (Schomer and Silva, 2010), have diminished the prospects of the traditional
21 Electroencephalography (EEG), the advent and development of digitized devices has impelled for a
22 revamping of this hundred years old technology. Their versatility, ease of use, temporal resolution, ease of
23 development and production, and its proliferation as consumer devices, are pushing EEG to become the
24 de-facto non invasive portable or ambulatory method to access and harness brain information (De Vos and
25 Debener, 2014).

26 A key contribution to this expansion has been the field of Brain Computer Interfaces (BCI) (Wolpaw and
27 E., 2012) which is the pursuit of the development of a new channel of communication particularly aimed to
28 persons affected by neurodegenerative diseases.

29 One noteworthy aspect of this novel communication channel is the ability to transmit information from
30 the Central Nervous System (CNS) to a computer device and from there use that information to control a
31 wheelchair (Carlson and del R. Millan, 2013), as input to a speller application (Guger et al., 2009), in a
32 Virtual Reality environment (Lotte et al., 2013) or as aiding tool in a rehabilitation procedure (Jure et al.,
33 2016). The holly grail of BCI is to implement a new complete and alternative pathway to restore lost
34 locomotion (Wolpaw and E., 2012).

35 EEG signals are remarkably complex and have been characterized as a multichannel non-stationary
36 stochastic process. Additionally, they have high variability between different subjects and even between
37 different moments for the same subject, requiring adaptive and co-adaptive calibration and learning
38 procedures (Clerc et al., 2016). Hence, this imposes an outstanding challenge that is necessary to overcome
39 in order to extract information from raw EEG signals.

40 BCI has gained mainstream public awareness with worldwide challenge competitions like
41 Cybathlon (Riener and Seward, 2014; Novak et al., 2018) and even been broadcasted during the inauguration
42 ceremony of the 2014 Soccer World Cup. New developments have overcome the out-of-the-lab high-bar
43 and they are starting to be used in real world environments (Guger et al., 2017; Huggins et al., 2016).
44 However, they still lack the necessary robustness, and its performance is well behind any other method of
45 human computer interaction, including any kind of detection of residual muscular movement (Clerc et al.,
46 2016).

47 A few works have explored the idea of exploiting the signal waveform to analyze the EEG signal.
48 In (Alvarado-González et al., 2016) an approach based on Slope Horizontal Chain Code is presented,
49 whereas in (Yamaguchi et al., 2009) a similar procedure was implemented based on Mathematical
50 Morphological Analysis. The seminal work of Bandt-Pompe Permutation Entropy (Berger et al., 2017) also
51 explores succinctly this idea as a basis to establish the time series ordinal patterns. In the article (Ramele
52 et al., 2016), the authors introduce a method for classification of rhythmic EEG events like Visual Occipital
53 Alpha Waves and Motor Imagery Rolandic Central μ Rhythms using the histogram of gradient orientations
54 of signal plots. Inspired in that work, we propose a novel application of the developed method to classify
55 and describe transient events, particularly the P300 Event Related Potential. The proposed approach is
56 based on the waveform analysis of the shape of the EEG signal, but using histogram of gradient orientations.
57 The method is built by mimicking what regularly electroencephalographers have been performing for
58 almost a century as it is described in (Hartman, 2005): visually inspecting raw signal plots.

59 This paper reports a method to, (1) describe a procedure to capture the shape of a waveform of an ERP
60 component, the P300, using histograms of gradient orientations extracted from images of signal plots, and
61 (2) outline the way in which this procedure can be used to implement an offline P300-based BCI Speller
62 application. Its validity is verified by offline processing two datasets, one of data from ALS patients and
63 another one from data of healthy subjects.

64 This article unfolds as follows: Section 2.1 is dedicated to explain the Feature Extraction method based
65 on Histogram of Gradient Orientations of the Signal Plot: Section 2.1.1 shows the preprocessing pipeline,
66 Section 2.1.2 describes the image generation of the signal plot, Section 2.1.3 presents the feature extraction
67 procedure while Section 2.1.4 introduces the Speller Matrix Letter Identification procedure. In Section 2.2,
68 the experimental protocol is expounded. Section 3 shows the results of applying the proposed technique. In
69 the final Section 4 we expose our remarks, conclusions and future work.

2 MATERIALS AND METHODS

The P300 (Farwell and Donchin, 1988; Knuth et al., 2006) is a positive deflection of the EEG signal which occurs around 300 ms after the onset of a rare and deviant stimulus that the subject is expected to attend. It is produced under the oddball paradigm (Wolpaw and E., 2012) and it is consistent across different subjects. It has a lower amplitude ($\pm 5\mu V$) compared to basal EEG activity, reaching a Signal to Noise Ratio (SNR) of around -15 db estimated based on the amplitude of the P300 response signal divided by the standard deviation of the background EEG activity (Hu et al., 2010). This signal can be used to implement a speller application by means of a Speller Matrix (Farwell and Donchin, 1988). This matrix is composed of 6 rows and 6 columns of numbers and letters. The subject can focus on one character of the matrix. Fig. 1 shows an example of the Speller Matrix used in the OpenVibe open source software (Renard et al., 2010), where the flashes of rows and columns provide the deviant stimulus required to elicit this physiological response. Each time a row or a column that contains the desired letter flashes, the corresponding synchronized EEG signal should also contain the P300 signature and by detecting it, the selected letter can be identified.

2.1 Feature Extraction from Signal Plots

In this section, the signal preprocessing, the method for generating images from signal plots, the feature extraction procedure and the Speller Matrix identification are described. Fig. 1 shows a scheme of the entire process.

2.1.1 Preprocessing Pipeline

The data obtained by the capturing device is digitalized and a multichannel EEG signal is constructed. The 6 rows and 6 columns of the Speller Matrix are intensified providing the visual stimulus. The twelve locations l are randomly permuted and they conform an intensification sequence. The whole set of twelve intensifications is repeated k_a times.

- **Signal Enhancement:** The preprocessing stage consists of the enhancement of the SNR of the P300 pattern above the level of basal EEG. The pipeline starts by applying a notch filter to the raw digital signal, a 4th degree 10 Hz lowpass Butterworth filter and finally a decimation with a Finite Impulse Response (FIR) filter of order 30 from the original sampling frequency down to 16 Hz (Lusienski et al., 2006).
- **Artifact Removal:** For every complete sequence of 12 intensifications of 6 rows and 6 columns, a basic artifact elimination procedure is implemented by removing the entire sequence when any signal deviates above/below $\pm 70\mu V$.
- **Segmentation:** For each of the 12 intensifications of one intensification sequence, a segment S_i^l of a window of t_{max} seconds of the multichannel signal is extracted, starting from the stimulus onset, corresponding to each row/column intensification l and to the intensification sequence i . As intensifications are randomly permuted, the segments are rearranged corresponding to row flickering, labeled 1-6, whereas those corresponding to column flickering are labeled 7-12. Two of these segments should contain the P300 ERP signature time-locked to the flashing stimulus, one for the row, and one for the column.
- **Signal Averaging:** The P300 ERP is deeply buried under background EEG so the standard approach to identify it is by point-to-point averaging the time-locked stacked signal segments. Hence the values which are not related to, and not time-locked to the onset of the stimulus are canceled out (Liang and Bougrain, 2008).

This last step determines the operation of any P300 Speller. In order to obtain an improved signal in terms of its SNR, repetitions of the sequence of row/column intensification are necessary. And, at the same time, as long as more repetitions are needed, the ability to transfer information faster is diminished, so there is a trade-off that must be acutely determined.

The procedure to obtain the point-to-point averaged signal goes as follows:

1. Highlight randomly the rows and columns from the matrix. There is one row and one column that should match the letter selected by the subject.
2. Repeat step 1 k_a times, obtaining the $1 \leq l \leq 12$ segments $S_1^l(n, c), \dots, S_{k_a}^l(n, c)$, of the EEG signal where the variables $1 \leq n \leq n_{max}$ and $1 \leq c \leq C$ correspond to sample points and channel, respectively. The parameter C is the number of available EEG channels whereas $n_{max} = F_s \cdot t_{max}$ is the segment length and F_s is the sampling frequency. The parameter k_a is the number of repetitions of intensifications and it is an input parameter of the algorithm.
3. Compute the Ensemble Average by

$$x^l(n, c) = \frac{1}{k_a} \sum_{i=1}^{k_a} S_i^l(n, c) \quad (1)$$

for $1 \leq n \leq n_{max}$ and for the channels $1 \leq c \leq C$. This provide an averaged signal $x^l(n, c)$ for the twelve locations.

2.1.2 Signal Plotting

Averaged signal segments are standardized and scaled by

$$\tilde{x}^l(n, c) = \left\lfloor \gamma \cdot \frac{(x^l(n, c) - \bar{x}^l(c))}{\hat{\sigma}^l(c)} \right\rfloor, \quad 1 \leq n \leq n_{max}, 1 \leq c \leq C \quad (2)$$

where $\gamma > 0$ is an input parameter of the algorithm and it is related to the image scale. In addition, $x^l(n, c)$ is the point-to-point averaged multichannel EEG signal for the sample point n and for channel c . Lastly,

$$\bar{x}^l(c) = \frac{1}{n_{max}} \sum_{n=1}^{n_{max}} x^l(n, c)$$

and

$$\hat{\sigma}^l(c) = \left(\frac{1}{n_{max} - 1} \sum_{n=1}^{n_{max}} (x^l(n, c) - \bar{x}^l(c))^2 \right)^{\frac{1}{2}}$$

are the mean and estimated standard deviation of $x^l(n, c)$, $1 \leq n \leq n_{max}$, for each channel c .

Consequently, for a pixel (z_1, z_2) , the image I^l is constructed according to

$$I^{(l,c)}(z_1, z_2) = \begin{cases} 255 & \text{if } z_1 = \gamma \cdot n; z_2 = \tilde{x}^l(n, c) + z^l(c) \\ 0 & \text{otherwise} \end{cases} \quad (3)$$

where $(z_1, z_2) \in \mathbb{N} \times \mathbb{N}$ iterate over the width (based on the length of the signal segment) and height (based on the peak-to-peak amplitude) of the newly created image, $1 \leq n \leq n_{max}$ and $1 \leq c \leq C$. The values



131 $z^l(c)$, are the location on the image where the signal's zero value has to be located in order to fit the entire
 132 signal within the image for each c .

$$z^l(c) = \left\lfloor \frac{\max_n \tilde{x}^l(n, c) - \min_n \tilde{x}^l(n, c)}{2} \right\rfloor - \left\lfloor \frac{\max_n \tilde{x}^l(n, c) + \min_n \tilde{x}^l(n, c)}{2} \right\rfloor \quad (4)$$

133 where the minimization and maximization are carried out for n varying between $1 \leq n \leq n_{max}$, and $\lfloor \cdot \rfloor$
 134 denote the rounding to the smaller nearest integer part of the number.

135 In order to complete the plot $I^{(l,c)}$ from the pixels, the Bresenham (Bresenham, 1965; Ramele et al.,
 136 2016) algorithm is used to interpolate straight lines between each pair of consecutive pixels.

137 2.1.3 Feature Extraction: Histogram of Gradient Orientations

138 For each generated image $I^{(l,c)}$, a keypoint \mathbf{p}_k is placed on a pixel (x_{p_k}, y_{p_k}) over the image plot and a
 139 window around the keypoint is considered. A local image patch of size $X_p \times X_p$ pixels is constructed by
 140 dividing the window in 16 blocks of size $3s$ each one, where s is the scale of the local patch and it is an
 141 input parameter of the algorithm. It is arranged in a 4×4 grid and the pixel \mathbf{p}_k is the patch center, thus
 142 $X_p = 12s$ pixels.

143 A local representation of the signal shape within the patch can be described by obtaining the gradient
 144 orientations on each of the 16 blocks $B_{i,j}$ and creating a histogram of gradients. This technique is based
 145 on Lowe's SIFT (Lowe, 2004) method, and it is biomimetically inspired in how the visual cortex detects
 146 shapes by analyzing orientations (Edelman et al., 1997). In order to calculate the histogram, the interval
 147 $[0, 360]$ of possible angles is divided in 8 bins, each one of 45 degrees.

148 Hence, for each spacial bin $0 \leq i, j \leq 3$, corresponding to the indexes of each block $B_{i,j}$, the orientations
 149 are accumulated in a 3-dimensional histogram h through the following equation:

$$h(\theta, i, j) = 3s \sum_{\mathbf{p} \in I} w_{ang}(\angle J(\mathbf{p}) - \theta) w_{ij} \left(\frac{\mathbf{p} - \mathbf{p}_k}{3s} \right) |J(\mathbf{p})| \quad (5)$$

150 where \mathbf{p} is a pixel from the image I , θ is the angle bin with $\theta \in \{0, 45, 90, 135, 180, 225, 270, 315\}$, $|J(\mathbf{p})|$
 151 is the norm of the gradient vector in the pixel \mathbf{p} and it is computed using finite differences and $\angle J(\mathbf{p})$ is the
 152 angle of the gradient vector. The scalar $w_{ang}(\cdot)$ and vector $w_{ij}(\cdot)$ functions are linear interpolations used
 153 by Lowe (2004) and Vedaldi and Fulkerson (2010) to provide a weighting contribution to eight adjacent
 154 bins. They are calculated as

$$w_{ij}(\mathbf{v}) = w(v_x - x_i)w(v_y - y_j) \quad (6)$$

155 with $0 \leq i, j \leq 3$ and

$$w_{ang}(\alpha) = \sum_{r \in [-1, 1]} w\left(\frac{8\alpha}{2\pi} + 8r\right) \quad (7)$$

156 where x_i and y_i are the spatial bin centers located in $x_i, y_i \in \{-\frac{3}{2}, -\frac{1}{2}, \frac{1}{2}, \frac{3}{2}\}$, $\mathbf{v} = (v_x, v_y)$ is a dummy
 157 vector variable and α a dummy scalar variable. On the other hand, r is an integer that can vary freely

158 between $[-1, 1]$ which allows the argument α to be unconstrained in terms of its values in radians. The
 159 interpolating function $w(\cdot)$ is defined as $w(z) = \max(0, |z| - 1)$.

160 These binning functions conform a trilinear interpolation that has a combined effect of sharing the
 161 contribution of each oriented gradient between their eight adjacent bins in a tridimensional cube in the
 162 histogram space, and zero everywhere else.

163 Lastly, the fixed value of 3 is a magnification factor which corresponds to the number of pixels per each
 164 block when $s = 1$. As the patch has 16 blocks and 8 bin angles are considered, for each location l and
 165 channel c a feature called *descriptor* $d^{(l,c)}$ of 128 dimension is obtained.

166 Fig. 2 shows an example of a patch and a scheme of the histogram computation. In (A) a plot of the
 167 signal and the patch centered around the keypoint is shown. In (B) the possible orientations on each patch
 168 are illustrated. Only the upper-left four blocks are visible. The first eight orientations of the first block, are
 169 labeled from 1 to 8 clockwise. The orientations of the second block $B_{1,2}$ are labeled from 9 to 16. This
 170 labeling continues left-to-right, up  down until the eight orientations for all the sixteen blocks are assigned.
 171 They form the corresponding  128 descriptor of 128 coordinates. Finally, in (C) an enlarged image plot is
 172 shown where the oriented gradient vector for each pixel can be seen.

173 2.1.4 Speller Matrix letter Identification

174 2.1.4.1 P300 ERP Extraction

175 Segments corresponding to row flickering are labeled 1-6, whereas those corresponding to column
 176 flickering are labeled 7-12. The extraction process has the following steps:

- 177 • **Step A:** First highlight randomly  the rows and columns from the matrix and obtain the Ensemble
 178 Average as detailed in steps 1, 2 and 3 in Section 2.1.1.
- 179 • **Step B:** Plot the signals $\tilde{x}^l(n, c)$, $1 \leq n \leq n_{max}$, $1 \leq c \leq C$, according Section 2.1.2 in order to
 180 generate the images $I^{(l,c)}$ for rows and columns.
- 181 • **Step C:** Obtain the descriptors $d^{(l,c)}$ for rows and columns from $I^{(l,c)}$ in accordance to the method
 182 described in Section 2.1.3.

183 2.1.4.2 Calibration

184 A trial, as defined by the BCI2000 platform (Schalk et al., 2004), is every attempt to select just one letter
 185 from the speller. A set of trials is used for calibration and once the calibration is complete it can be used to
 186 identify new letters from new trials.

187 During the calibration phase, two descriptors $d^{(l,c)}$ are extracted for each available channel for the
 188 calibration trials, corresponding a previously  own chosen letter. These descriptors are the P300 templates,
 189 grouped together in a  template set called T . The set is constructed using the steps described in Section
 190 2.1.1 and the steps A, B and C of the P300 ERP extraction process.

191 Additionally, the best performing channel, bpc is identified based on the the channel where the best
 192 Character Recognition Rate is obtained.

193 2.1.4.3 Letter identification

194 In order to identify the selected letter, the template set T is used as a database. Thus, new descriptors are
 195 computed and they are compared against the descriptors belonging to the calibration template set T .

- 196 • **Step C:** Match to the calibration template T by computing 

$$\hat{row} = \arg \min_{l \in \{1, \dots, 6\}} \sum_{q \in N_T(d^{(l,bpc)})} \|q - d^{(l,bpc)}\|^2 \quad (8)$$

197 and

$$\hat{col} = \arg \min_{l \in \{7, \dots, 12\}} \sum_{a \in N_T(d^{(l,bpc)})} \|q - d^{(l,bpc)}\|^2 \quad (9)$$

198 where $N_T(d^l)$ is defined as $N_T(d^l) = \{d \in \text{[redacted]} \mid d \text{ is the } k\text{-nearest neighbor of } d^l\}$ for the best performing channel. This set is obtained by sorting all the elements in [redacted] based on distances between them and d^l , choosing the k with smaller values, with k a parameter of the algorithm. This procedure is based on 199 200 201 the k-NBNN algorithm (Boiman et al., 2008).

202 By computing the aforementioned equations, the letter of the matrix can be determined from the intersection 203 of the row \hat{row} and column \hat{col} . Figure 3 shows a scheme of this process.

204 2.2 Experimental Protocol

205 To verify the validity of the proposed framework and method, the public dataset 008-2014 (Riccio et al., 206 2013) published on the BNCI-Horizon website (Brunner et al., 2014) by IRCCS Fondazione Santa Lucia, 207 is used. Additionally, an own dataset with the same experimental conditions is generated. Both of them are 208 utilized to perform an offline BCI Simulation to decode the spelled words from the provided signals.

209 The algorithm is implemented using VLFeat (Vedaldi and Fulkerson, 2010) Computer Vision libraries on 210 MATLAB V2014a (Mathworks Inc., Natick, MA, USA).

211 In the following sections the characteristics of the datasets and parameters of the identification algorithm 212 are described.

213 2.2.1 P300 ALS Public Dataset

214 The experimental protocol used to generate this dataset is explained in (Riccio et al., 2013) but can 215 be summarized as follows: 8 subjects with confirmed diagnoses but on different stages of ALS disease, 216 were recruited and accepted to perform the experiments. The Visual P300 detection task designed for this 217 experiment consisted of spelling 7 words of 5 letters each, using the traditional P300 Speller Matrix (Farwell 218 and Donchin, 1988). The flashing of rows and columns provide the deviant stimulus required to elicit this 219 physiological response. The first 3 words are used for calibration and the remaining 4 words, for testing 220 with visual feedback. A trial, as defined by the BCI2000 platform (Schalk et al., 2004), is every attempt to 221 select a letter from the speller. It is composed of signal segments corresponding to $k_a = 10$ repetitions of 222 flashes of 6 rows and $k_a = 10$ repetitions of flashes of 6 columns of the matrix, yielding 120 repetitions. 223 Flashing of a row or a column is performed for 0.125 s, following by a resting period (i.e. inter-stimulus 224 interval) of the same length. After 120 repetitions an inter-trial pause is included before resuming with the 225 following letter.

226 The recorded dataset was sampled at 256 Hz and it consisted of a scalp multichannel EEG signal for 227 electrode channels Fz, Cz, Pz, Oz, P3, P4, PO7 and PO8, identified according to the 10-20 International 228 System, for each one of the 8 subjects. The recording device was a research-oriented digital EEG device 229 (g.Mobilab, g.Tec, Austria) and the data acquisition and stimuli delivery were handled by the BCI2000 230 open source software (Schalk et al., 2004).

231 In order to assess and verify the identification of the P300 response, subjects are instructed to perform a
 232 copy-spelling task. They have to fix their attention to successive letters for copying a previously determined
 233 set of words, in contrast to a free-running operation of the speller where each user decides on its own what
 234 letter to choose.

235 **2.2.2 P300 for healthy subjects**

236 We replicate the same experiment on healthy subjects (Ramele et al., 2017) using a wireless digital EEG
 237 device (g.Nautilus, g.Tec, Austria). The experimental conditions are the same as those used for the previous
 238 dataset, as detailed in section 2.2.1.

239 Participants are recruited voluntarily and the experiment is conducted anonymously in accordance with
 240 the Declaration of Helsinki published by the World Health Organization. No monetary compensation
 241 is handed out and all participants agree and sign a written informed consent. This study is approved
 242 by the *Departamento de Investigación y Doctorado, Instituto Tecnológico de Buenos Aires (ITBA)*. All
 243 healthy subjects have normal or corrected-to-normal vision and no history of neurological disorders. The
 244 experiment is performed with 8 subjects, 6 males, 2 females, 6 right-handed, 2 left-handed, average age
 245 29.00 years, standard deviation 11.56 years, range 20-56 years.

246 EEG data is collected in a single recording session. Participants are seated in a comfortable chair, with
 247 their vision aligned to a computer screen located one meter in front of them. The handling and processing
 248 of the data and stimuli is conducted by the OpenVibe platform (Renard et al., 2010).

249 Gel-based active electrodes (g.LADYbird, g.Tec, Austria) are used on the same locations Fz, Cz, Pz,
 250 Oz, P3,P4, PO7 and PO8. Reference is set to the right ear lobe and ground is preset as the AFz position.
 251 Sampling frequency is slightly different, and is set to 250 Hz, which is the closest possible to the one used
 252 with the other dataset.

253 **2.2.3 Parameters**

254 The patch size is $X_P = 12s \times 12s$ pixels, where s is the scale  local patch and it is an input parameter
 255 of the algorithm. The P300 event can have a span of 400 ms and its amplitude can reach $10\mu V$ (Rao, 2013).
 256 Hence it is necessary to utilize a signal segment of size $t_{max} = 1$ second and a size patch X_P that could
 257 capture an entire transient event. With this purpose in consideration, the s value election is essential.

258 We propose the Equations 10 and 11 to compute the scale value in horizontal and vertical directions,
 259 respectively.

$$s_x = \frac{\gamma \cdot \lambda \cdot F_s}{12} \quad (10)$$

$$s_y = \frac{\gamma \cdot \Delta\mu V}{12} \quad (11)$$

260 where λ is the length  in seconds covered by the patch, F_s is the sampling frequency of the EEG signal
 261 (downsampled to  Hz) and $\Delta\mu V$ corresponds to the amplitude in microvolts that can be covered by the
 262 height of the patch. The geometric structure of the patch forces a squared configuration, then we discerned
 263 that by using $s = s_x = s_y = 3$ and $\gamma = 4$, the local patch and the descriptor can identify events of 
 264 of amplitude, with a span of $\lambda = 0.56$  seconds. This also determines that 1 pixel represents $\frac{1}{\gamma} = \frac{1}{4}\mu V$
 265 on the vertical direction and $\frac{1}{F_s \cdot \gamma} = \frac{1}{64}$  seconds on the horizontal direction. Descriptors p_k are located
 266 at $(x_{p_k}, y_{p_k}) = (0.55F_s \cdot \gamma, z^l(c)) = (35, z^l(c))$ for the corresponding channel c and location l (see  Eq. 4).

267 In this way the whole transient event is captured. Figure 4 shows a patch of a signal plot covering the
268 complete amplitude (vertical direction) and the complete span of the signal event (horizontal direction).

269 Lastly, the number of channels C is equal to 8 for both datasets, and \square number of intensification
270 sequences k_a is statically assigned to 10. The parameter k used to construct the set $N_T(d^l)$ is assigned to
271 $k = 7$, which was found empirically to achieve better results. In addition, the norm used on Equations 8
272 and 9 is the cosine norm, and descriptors are normalized to $[-1, 1]$.

3 RESULTS

273 Table 1 shows the results of applying the algorithm to the subjects of the public dataset of ALS patients.
274 The percentage of correctly spelled letters is calculated while performing an offline BCI Simulation. From
275 the seven words for each subject, the first three are used as calibration, and the remaining four for testing.
276 The best performing channel bpc is informed as well. The target ratio is 1 : 36; hence chance level is
277 2.8%. It can be observed that the best performance of the letter identification method is reached in various
278 channels depending on the subject been studied.

279 The Information Transfer Rate (ITR), or Bit Transfer Rate (BTR), in the case of reactive BCIs (Wolpaw
280 and E., 2012) depends on the amount of signal averaging required to transmit a valid and robust selection.
281 Fig. 5 shows the performance curves for varying intensification sequences. It can be noticed that the
282 percentage of correctly identified letters depends on the number of intensification sequences k_a that are
283 used to obtain the averaged signal. Moreover, when the number of intensification sequences tend to 1, which
284 corresponds to single-intensification character recognition, the performance is reduced. As mentioned
285 before, the SNR of the P300 obtained from only one segment is very low and the shape of its P300
286 component is not very well defined.

287 In Table 3 results obtained for 8 healthy subjects are shown. The obtained performance were slightly
288 inferior than those obtained for ALS patients but well above chance level.

289 In both tables results for character recognition rates using single channel signals with the SVM classifier
290 and using a feature based on Permutation Entropy and classified by SVM (PE+SVM) are also shown.
291 The PE algorithm, which is also based on a time-domain description of the waveform, was implemented
292 according to (Unakafova and Keller, 2013) and its parameters were adjusted as stated by (Zanin et al.,
293 2012), with an *order* of 2 and a *sliding window* of size 10. The SVM classifier, on the other hand, was
294 configured to use a linear kernel. Moreover, in Tables 2 and 4 performance for letter identification rates
295 for the SWLDA algorithm are expounded. The feature was obtained by concatenating all the channels
296 (Krusienski et al., 2006) and the SWLDA algorithm is used in accordance to the publishers of the ALS
297 dataset (Riccio et al., 2013). The rate obtained for both datasets is slightly improved in relation to SWLDA.

298 The P300 ERP consists of two overlapping components: the P3a and P3b, the former with frontocentral
299 distribution while the later stronger on centroparietal region (Polich, 2007). Hence, the standard practice is
300 to find the stronger response on the central channel Cz (Riccio et al., 2013). However, Krusienski et al.
301 (2006) show that the response may also arise in occipital regions. We found that by analyzing only the
302 waveforms, occipital channels PO8 and PO7 show higher performances for some subjects.

303 As subjects have varying *latencies* and *amplitudes* of their P300 components, they also have a varying
304 stability of the *shape* of the generated ERP (Nam et al., 2010). Figure 6 shows the P300 templates patches
305 for patients 8 and 3 from the dataset of ALS patients. It can be discerned that in coincidence with the

306 performance results, the P300 signature is more clear and consistent for subject 8 (A) while for subject 3
307 (B) the characteristic pattern is more difficult to perceive.

308 Additionally, the stability of the P300 component waveform has been extensively studied in patients
309 with ALS (Sellers et al., 2006; Madarame et al., 2008; Nijboer and Broermann, 2009; Mak et al., 2012;
310 McCane et al., 2015) where it was found that these patients have a stable P300 component, which were
311 also sustained across different sessions. In line with these results we do not find evidence of a difference in
312 terms of the performance obtained for the group of patients with ALS and the healthy group of volunteers.
313 Particularly, the best performance is obtained for a subject from the ALS dataset for which, based on visual
314 observation, the shape of they P300 component is consistently identified.

315 It is important to remark that when applied to binary images obtained from signal plots, the feature
316 extraction method described in Section 2.1.3 generates sparse descriptors. Under this subspace we found
317 that using the cosine metric yielded a significant performance improvement. On the other hand, the unary
318 classification scheme based on the NBNN algorithm proved very beneficial for the P300 Speller Matrix.
319 This is due to the fact that this approach solves the unbalance dataset problem which is inherent to the
320 oddball paradigm (Tibon and Levy, 2015).

4 DISCUSSION

321 Among other applications of Brain Computer Interfaces, the goal of the discipline is to provide
322 communication assistance to people affected by neuro-degenerative diseases, who are the most likely
323 population to benefit from BCI systems and EEG processing and analysis.

324 In this work, a method to detect transient P300 components from EEG signals based on their waveform
325 characterization in digital time-space, is presented. Additionally, its validity is evaluated using a public
326 dataset of ALS patients and an own dataset of healthy subjects.

327 This method has the advantage that shapes of waveforms can be analyzed in an objective way. We
328 observed that the shape of the P300 component is more stable in occipital channels, where the performance
329 for identifying letters is higher. We additionally verified that ALS P300 signatures are stable in comparison
330 to those of healthy subjects. Further work should be conducted over larger samples to cross-check the
331 validity of these results.

332 We believe that the use of descriptors based on histogram of gradient orientation, presented in this work,
333 can also be utilized for deriving a shape metric in the space of the P300 signals which can complement
334 other metrics based on time-domain as those defined by Mak et al. (2012). It is important to notice
335 that the analysis of waveform shapes is usually performed in a qualitative approach based on visual
336 inspection (Sellers et al., 2006).

337 The goal of this work is to answer the question if a P300 component could be solely determined by
338 inspecting automatically their waveforms. We conclude affirmatively, though two very important issues
339 still remain:

340 First, the stability of the P300 in terms of its shape is crucial: the averaging procedure, montages, the
341 signal to noise ratio and spatial filters all of them are non-physiological factors that affect the stability
342 of the shape of the P300 ERP. We tested a preliminary approach to assess if the morphological shape of
343 the P300 can be stabilized by applying different latency shifts to segments and we verified that there is a
344 better performance when a correct segment alignment is applied. We also applied Dynamic Time Warping

345 (DTW) (Casarotto et al., 2005) but we were unable to find a substantial improvement. Further work to
346 study the stability of the P300 signature component needs to be addressed.

347 The second problem is the amplitude variation of the P300. We propose a solution by standardizing the
348 signal, shown in Eq. 2. It has the effect of normalizing the peak-to-peak amplitude, moderating its variation.
349 It has also the advantage of reducing noise that was not reduced by the averaging procedure. It is important
350 to remark that the averaged signal variance depends on the number of segments used to compute it (Van
351 Drongelen, 2006). The standardizing process converts the signal to unit signal variance which makes it
352 independent of the number k_a of signals averaged. Although this is initially an advantageous approach, the
353 standardizing process reduces the amplitude of any significant P300 complex diminishing its automatic
354 interpretation capability.

355 In our opinion, the best benefit of the presented method is that a closer collaboration with physicians can
356 be fostered, since this procedure intent to imitate human visual observation. Automatic classification of
357 patterns in EEG that are specifically identified by their shapes like K-Complex, Vertex Waves, Positive
358 Occipital Sharp Transient (Hartman, 2005) are a prospect future work to be considered. We are currently
359 working in unpublished material analyzing K-Complex components that could eventually provide assistance
360 to physicians to locate these EEG patterns, specially in long recording periods, frequent in sleep research.
361 Additionally, it can be used for artifact removal which is performed on many occasions by visually
362 inspecting signals. This is due to the fact that the descriptors are a direct representation of the shape
363 of signal waveforms. In line with these applications, it can be used to build a database (Chavarriaga
364 et al., 2017) of quantitative representations of waveforms and improve atlases (Hartman, 2005), which are
365 currently based on qualitative descriptions of signal shapes.

CONFLICT OF INTEREST STATEMENT

366 The authors declare that the research was conducted in the absence of any commercial or financial
367 relationships that could be construed as a potential conflict of interest.

AUTHOR CONTRIBUTIONS

368 This work is part of the PhD thesis of RR which is directed by JS and codirected by AV.

FUNDING

369 This project was supported by the ITBACyT-15 funding program issued by ITBA University from Buenos
370 Aires, Argentina.

REFERENCES

- 371 Alvarado-González, M., Garduño, E., Bribiesca, E., Yáñez-Suárez, O., and Medina-Bañuelos, V. (2016).
372 P300 Detection Based on EEG Shape Features. *Computational and Mathematical Methods in Medicine*,
373 1–14doi:10.1155/2016/2029791
- 374 Berger, S., Schneider, G., Kochs, E., and Jordan, D. (2017). Permutation Entropy: Too Complex a Measure
375 for EEG Time Series? *Entropy 2017, Vol. 19, Page 692* 19, 692. doi:10.3390/E19120692
- 376 Boiman, O., Shechtman, E., and Irani, M. (2008). In defense of nearest-neighbor based image classification.
377 *26th IEEE Conference on Computer Vision and Pattern Recognition, CVPR* doi:10.1109/CVPR.2008.
378 4587598

- 379 Bresenham, J. E. (1965). Algorithm for computer control of a digital plotter. *IBM Systems Journal* 4,
380 25–30
- 381 Brunner, C., Blankertz, B., Cincotti, F., Kübler, A., Mattia, D., Miralles, F., et al. (2014). BNCI Horizon
382 2020 – Towards a Roadmap for Brain / Neural Computer Interaction. *Lecture Notes in Computer Science*
383 8513, 475–486
- 384 Carlson, T. and del R. Millan, J. (2013). Brain-controlled wheelchairs: A robotic architecture. *IEEE*
385 *Robotics & Automation Magazine* 20, 65–73. doi:10.1109/MRA.2012.2229936
- 386 Casarotto, S., Bianchi, A., Cerutti, S., and Chiarenza, G. (2005). Dynamic time warping in the analysis of
387 event-related potentials. *IEEE Engineering in Medicine and Biology Magazine* 24, 68–77. doi:10.1109/
388 MEMB.2005.1384103
- 389 Chavarriaga, R., Fried-Oken, M., Kleih, S., Lotte, F., and Scherer, R. (2017). Heading for new shores!
390 Overcoming pitfalls in BCI design. *Brain-Computer Interfaces* 4, 60–73. doi:10.1080/2326263X.2016.
391 1263916
- 392 Clerc, M., Bougrain, L., and Lotte, F. (2016). *Brain-computer interfaces, Technology and applications*
393 2(Cognitive Science) (ISTE Ltd. and Wiley)
- 394 De Vos, M. and Debener, S. (2014). Mobile EEG: Towards brain activity monitoring during natural action
395 and cognition. *International Journal of Psychophysiology* 91, 1–2. doi:10.1016/j.ijpsycho.2013.10.008
- 396 Edelman, S., Intrator, N., and Poggio, T. (1997). Complex cells and object recognition
- 397 Farwell, L. A. and Donchin, E. (1988). Talking off the top of your head: toward a mental prosthesis utilizing
398 event-related brain potentials. *Electroencephalography and clinical neurophysiology* 70, 510–23
- 399 Guger, C., Allison, B. Z., and Lebedev, M. A. (2017). Introduction. In *Brain Computer Interface Research: A State of the Art Summary* 6 (Springer, Cham). 1–8. doi:10.1007/978-3-319-64373-1_1
- 400 Guger, C., Daban, S., Sellers, E., Holzner, C., Krausz, G., Carabalona, R., et al. (2009). How many people
401 are able to control a P300-based brain-computer interface (BCI)? *Neuroscience Letters* 462, 94–98.
402 doi:10.1016/j.neulet.2009.06.045
- 403 Hartman, a. L. (2005). *Atlas of EEG Patterns*, vol. 65 (Lippincott Williams & Wilkins). doi:10.1212/01.
404 wnl.0000174180.41994.39
- 405 Hu, L., Mouraux, A., Hu, Y., and Iannetti, G. D. (2010). A novel approach for enhancing the signal-to-noise
406 ratio and detecting automatically event-related potentials (ERPs) in single trials. *NeuroImage* 50, 99–111.
407 doi:10.1016/j.neuroimage.2009.12.010
- 408 Huggins, J. E., Alcaide-Aguirre, R. E., and Hill, K. (2016). Effects of text generation on P300 brain-
409 computer interface performance. *Brain-Computer Interfaces* 3, 112–120. doi:10.1080/2326263X.2016.
410 1203629
- 411 Jure, F., Carrere, L., Gentiletti, G., and Tabernig, C. (2016). BCI-FES system for neuro-rehabilitation of
412 stroke patients. *Journal of Physics: Conference Series* 705, 1–8. doi:10.1088/1742-6596/705/1/012058
- 413 Knuth, K. H., Shah, A. S., Truccolo, W. A., Ding, M., Bressler, S. L., and Schroeder, C. E. (2006).
414 Differentially variable component analysis: Identifying multiple evoked components using trial-to-trial
415 variability. *Journal of Neurophysiology* 95, 3257–3276. doi:10.1152/jn.00663.2005
- 416 Krusienski, D. J., Sellers, E. W., Cabestaing, F., Bayoudh, S., McFarland, D. J., Vaughan, T. M., et al.
417 (2006). A comparison of classification techniques for the P300 Speller. *Journal of Neural Engineering*
418 3, 299–305. doi:10.1088/1741-2560/3/4/007
- 419 Liang, N. and Bougrain, L. (2008). Averaging techniques for single-trial analysis of oddball event-related
420 potentials. *4th International Brain-Computer* , 1–6
- 421

- 422 Lotte, F., Faller, J., Guger, C., Renard, Y., Pfurtscheller, G., Lécuyer, A., et al. (2013). *Combining BCI*
423 *with Virtual Reality: Towards New Applications and Improved BCI* (Berlin, Heidelberg: Springer Berlin
424 Heidelberg). 197–220. doi:10.1007/978-3-642-29746-5_10
- 425 Lowe, G. (2004). SIFT - The Scale Invariant Feature Transform. *International Journal* 2, 91–110
- 426 Madarame, T., Tanaka, H., Inoue, T., Kamata, M., and Shino, M. (2008). The development of a brain
427 computer interface device for amyotrophic lateral sclerosis patients. In *Conference Proceedings - IEEE*
428 *International Conference on Systems, Man and Cybernetics* (IEEE), 2401–2406. doi:10.1109/ICSMC.
429 2008.4811654
- 430 Mak, J. N., McFarland, D. J., Vaughan, T. M., McCane, L. M., Tsui, P. Z., Zeitlin, D. J., et al. (2012). EEG
431 correlates of P300-based brain-computer interface (BCI) performance in people with amyotrophic lateral
432 sclerosis. *Journal of Neural Engineering* 9. doi:10.1088/1741-2560/9/2/026014
- 433 McCane, L. M., Heckman, S. M., McFarland, D. J., Townsend, G., Mak, J. N., Sellers, E. W., et al.
434 (2015). P300-based brain-computer interface (BCI) event-related potentials (ERPs): People with
435 amyotrophic lateral sclerosis (ALS) vs. age-matched controls. *Clinical Neurophysiology* 126, 2124–2131.
436 doi:10.1016/j.clinph.2015.01.013
- 437 Nam, C. S., Li, Y., and Johnson, S. (2010). Evaluation of P300-based brain-computer interface in real-
438 world contexts. *International Journal of Human-Computer Interaction* 26, 621–637. doi:10.1080/
439 10447311003781326
- 440 Nijboer, F. and Broermann, U. (2009). Brain Computer Interfaces for Communication and Control in
441 Locked-in Patients. In *Graimann B., Pfurtscheller G., Allison B. (eds) Brain-Computer Interfaces. The*
442 *Frontiers Collection*. (Springer Berlin Heidelberg). 185–201. doi:10.1007/978-3-642-02091-9_11
- 443 Novak, D., Sigrist, R., Gerig, N. J., Wyss, D., Bauer, R., Gotz, U., et al. (2018). Benchmarking brain-
444 computer interfaces outside the laboratory: The cybathlon 2016. *Frontiers in Neuroscience* 11, 756.
445 doi:10.3389/fnins.2017.00756
- 446 Polich, J. (2007). Updating P300: An integrative theory of P3a and P3b. *Clinical Neurophysiology* 118,
447 2128–2148. doi:10.1016/j.clinph.2007.04.019
- 448 Ramele, R., Villar, A. J., and Santos, J. M. (2016). BCI classification based on signal plots and SIFT
449 descriptors. In *4th International Winter Conference on Brain-Computer Interface, BCI 2016* (Yongpyong:
450 IEEE), 1–4. doi:10.1109/IWW-BCI.2016.7457454
- 451 [Dataset] Ramele, R., Villar, A. J., and Santos, J. M. (2017). P300-dataset rrid scr_015977. <https://www.kaggle.com/rramele/p300samplingdataset>
- 453 Rao, R. P. N. (2013). *Brain-Computer Interfacing: An Introduction* (New York, NY, USA: Cambridge
454 University Press)
- 455 Renard, Y., Lotte, F., Gibert, G., Congedo, M., Maby, E., Delannoy, V., et al. (2010). OpenViBE: An
456 Open-Source Software Platform to Design, Test, and Use Brain–Computer Interfaces in Real and Virtual
457 Environments. *Presence: Teleoperators and Virtual Environments* 19, 35–53. doi:10.1162/pres.19.1.35
- 458 Riccio, A., Simione, L., Schettini, F., Pizzimenti, A., Inghilleri, M., Belardinelli, M. O., et al. (2013).
459 Attention and P300-based BCI performance in people with amyotrophic lateral sclerosis. *Frontiers in*
460 *Human Neuroscience* 7, 732. doi:10.3389/fnhum.2013.00732
- 461 Riener, R. and Seward, L. J. (2014). Cybathlon 2016. *2014 IEEE International Conference on Systems,*
462 *Man, and Cybernetics (SMC)*, 2792–2794doi:10.1109/SMC.2014.6974351
- 463 Schalk, G., McFarland, D. J., Hinterberger, T., Birbaumer, N., and Wolpaw, J. R. (2004). BCI2000: a
464 general-purpose brain-computer interface (BCI) system. *IEEE transactions on bio-medical engineering*
465 51, 1034–43. doi:10.1109/TBME.2004.827072

- 466 Schomer, D. L. and Silva, F. L. D. (2010). *Niedermeyer's Electroencephalography: Basic Principles, Clinical Applications, and Related Fields* (Walters Klutter -Lippincott Williams & Wilkins)
- 468 Sellers, E. W., Kübler, A., and Donchin, E. (2006). Brain-computer interface research at the University of South Florida cognitive psychophysiology laboratory: The P300 speller. *IEEE Transactions on Neural Systems and Rehabilitation Engineering* 14, 221–224. doi:10.1109/TNSRE.2006.875580
- 471 Tibon, R. and Levy, D. A. (2015). Striking a balance: analyzing unbalanced event-related potential data. *Frontiers in psychology* 6, 555. doi:10.3389/fpsyg.2015.00555
- 473 Unakafova, V. and Keller, K. (2013). Efficiently Measuring Complexity on the Basis of Real-World Data. *Entropy* 15, 4392–4415. doi:10.3390/e15104392
- 475 Van Drongelen, W. (2006). *Signal processing for neuroscientists: an introduction to the analysis of physiological signals* (Academic press)
- 477 Vedaldi, A. and Fulkerson, B. (2010). VLFeat - An open and portable library of computer vision algorithms. *Design* 3, 1–4. doi:10.1145/1873951.1874249
- 479 Wolpaw, J. and E., W. (2012). *Brain-Computer Interfaces: Principles and Practice* (Oxford University Press)
- 481 Yamaguchi, T., Fujio, M., Inoue, K., and Pfurtscheller, G. (2009). Design method of morphological structural function for pattern recognition of EEG signals during motor imagery and cognition. In *Fourth International Conference on Innovative Computing, Information and Control (ICICIC)*. 1558–1561. doi:10.1109/ICICIC.2009.161
- 485 Zanin, M., Zunino, L., Rosso, O. A., and Papo, D. (2012). Permutation entropy and its main biomedical and econophysics applications: A review. *Entropy* 14, 1553–1577. doi:10.3390/e14081553

Table 1. Character recognition rates while performing an offline BCI Simulation for the best performing channel for each subject of the public dataset of ALS patients using the Histogram of Gradients (HIST). The spelled words are *GATTO*, *MENTE*, *VIOLA* and *REBUS*. Performance rates using single channel signals with the SVM classifier and using a feature obtained with Permutation Entropy (PE) and classified by SVM are also shown for comparison.

Participant	BPC	HIST	BPC	SVM	BPC	PE+SVM
1	Cz	35%	Cz	15%	P3	05%
2	Fz	85%	PO8	25%	PO8	15%
3	Cz	25%	Fz	05%	P3	05%
4	PO8	55%	Oz	05%	Oz	10%
5	PO7	40%	P3	25%	PO8	15%
6	PO7	60%	PO8	20%	Fz	10%
7	PO8	80%	Fz	30%	Fz	10%
8	PO7	95%	PO7	85%	PO8	25%

Table 2. Character recognition rates for the public dataset of ALS patients using the Histogram of Gradient (HIST) and performance rates obtained by the popular SWLDA with a multichannel concatenated feature.

Participant	BPC	Character Recognition Rates	
		HIST	SWLDA
1	Cz	35%	45%
2	Fz	85%	30%
3	Cz	25%	65%
4	PO8	55%	40%
5	PO7	40%	35%
6	PO7	60%	35%
7	PO8	80%	60%
8	PO7	95%	90%

Table 3. Percentage of correctly predicted letters while performing an offline BCI Simulation for the best performing channel for each subject of the own dataset. The spelled words are *MANSO*, *CINCO*, *JUEGO* and *QUESO*. Performance rates using single channel signals with the SVM classifier and using a feature obtained with Permutation Entropy (PE) and classified by SVM are also shown for comparison.

Participant	BPC	HIST	BPC	SVM	BPC	PE+SVM
1	Oz	40%	Cz	10%	PO7	10%
2	PO7	30%	Cz	05%	Fz	05%
3	P4	40%	P3	10%	Fz	00%
4	P4	45%	P4	35%	Cz	10%
5	P4	60%	P3	10%	Fz	00%
6	Pz	50%	P4	25%	Cz	10%
7	PO7	70%	P3	30%	P3	10%
8	P4	50%	PO7	10%	Fz	05%

Table 4. Percentage of correctly predicted letters while performing an offline BCI Simulation for the best performing channel for each subject of the own dataset. Results obtained with the SWLDA algorithm with a multichannel concatenated feature are presented.

Participant	BPC	Character Recognition Rates	
		HIST	SWLDA
1	Oz	40%	65%
2	PO7	30%	15%
3	P4	40%	50%
4	P4	45%	40%
5	P4	60%	30%
6	Pz	50%	35%
7	PO7	70%	25%
8	P4	50%	35%

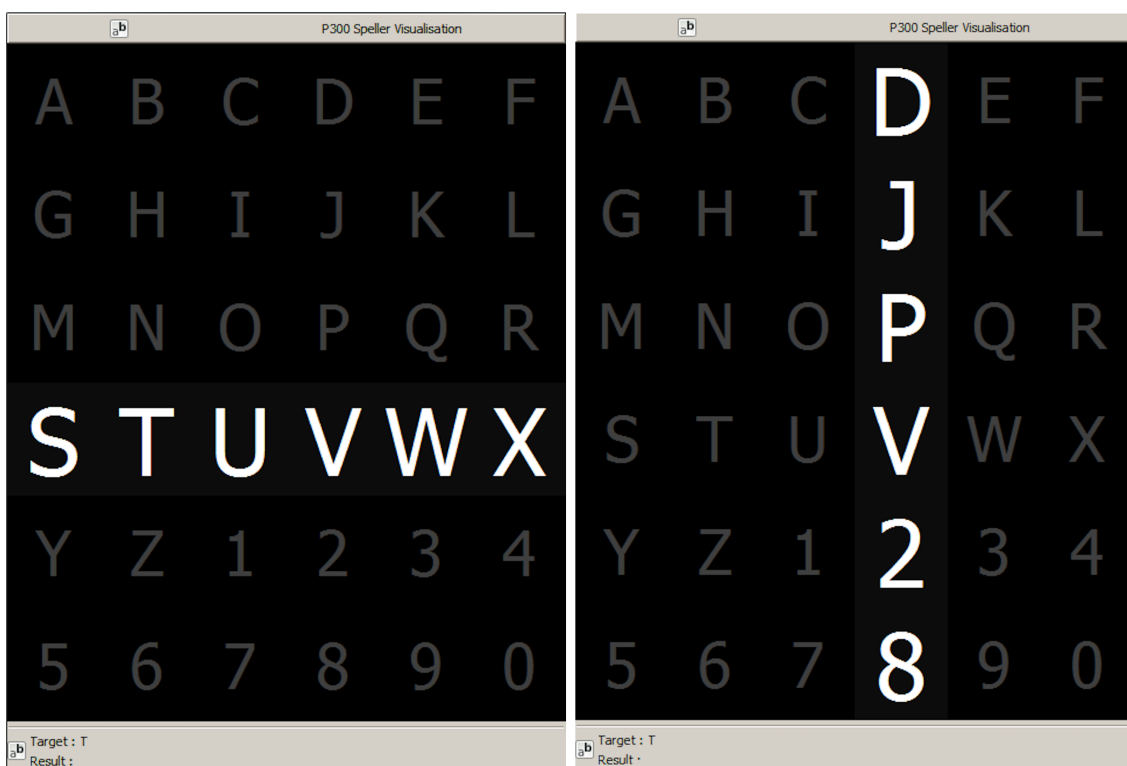


Figure 1. Example of the 6×6 Speller Matrix used in the study. Rows and columns flash in random permutations. 

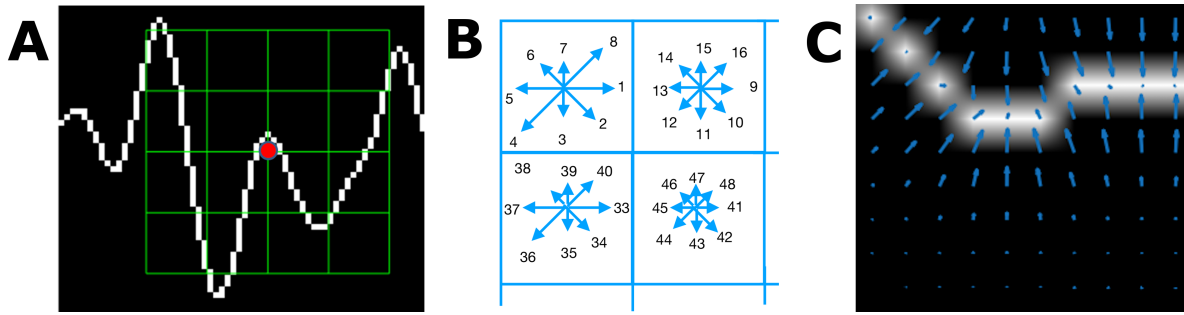


Figure 2. (A) Example of a plot of the signal, a keypoint and the corresponding patch. (B) A scheme of the orientation's histogram computation. Only the upper-left four blocks are visible. The first eight orientations of the first block, are labeled from 1 to 8 clockwise. The orientation of the second block $B_{1,2}$ is labeled from 9 to 16. This labeling continues left-to-right, up-down until the eight orientations for all the sixteen blocks are assigned. They form the corresponding p_k -descriptor of 128 coordinates. The length of each arrow represent the value of the histogram on each direction for each block. (C) Vector field of oriented gradients. Each pixel is assigned an orientation and magnitude calculated using finite differences.

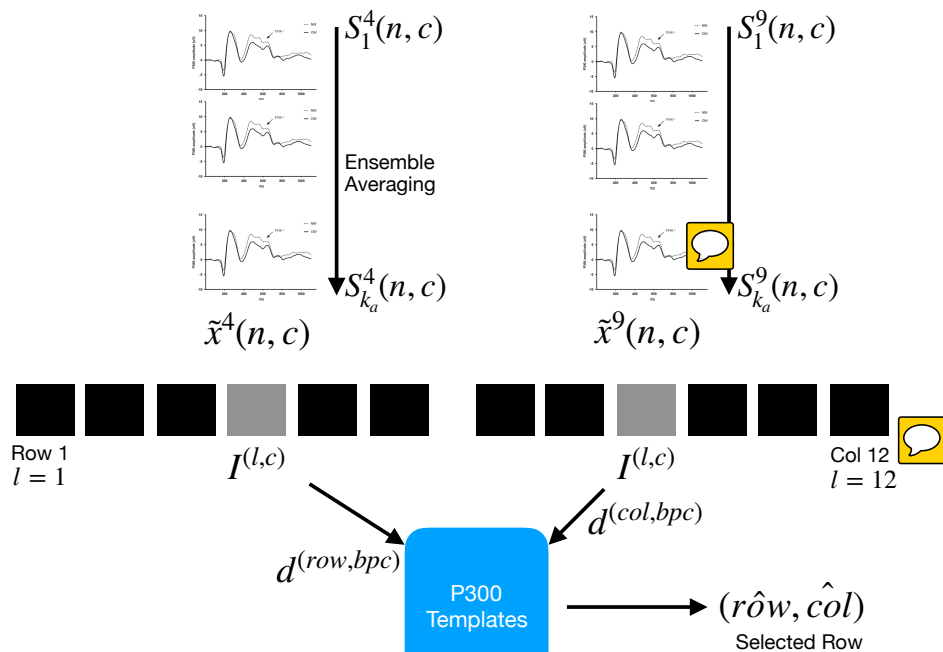


Figure 3. Segments S_i are averaged for the 6 rows and 6 columns. From the averaged signal, the image of the signal plot is generated and each descriptor is computed. By comparing each descriptor against the set of templates, the P300 ERP can be detected, and finally the desired letter from the matrix can be inferred.

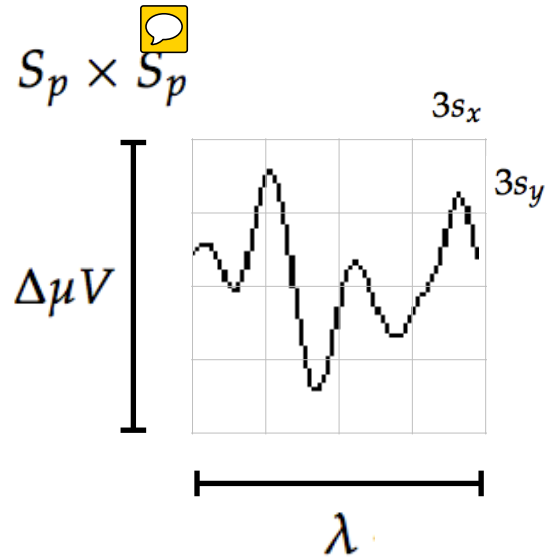


Figure 4. The scale of local patch is selected in order to capture the whole transient event. The size of the patch is $X_p \times X_p$ pixels. The vertical size consists of 4 blocks of size $3s_y$ pixels which is high enough as to contain the signal $\Delta\mu V$, the peak-to-peak amplitude of the transient event. The horizontal size includes 4 blocks of $3s_x$ and covers the entire duration in seconds of the transient signal event, λ .

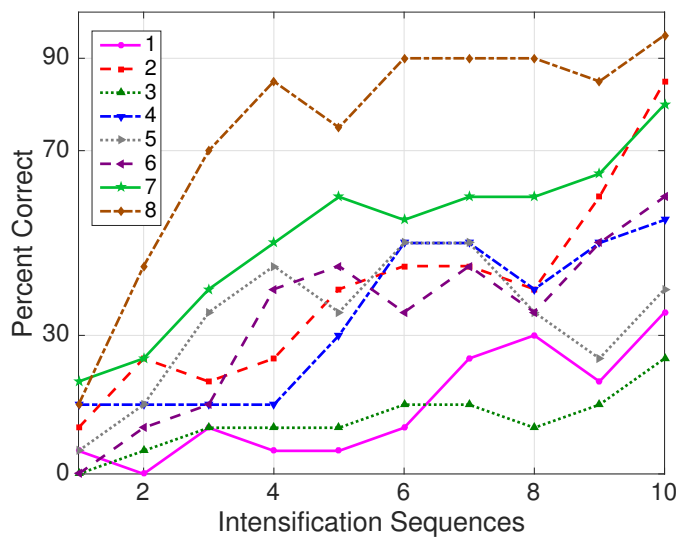


Figure 5. Performance curves for the eight subjects included in the dataset of ALS patients. Three out of eight subjects achieved the necessary performance to implement a valid P300 speller.

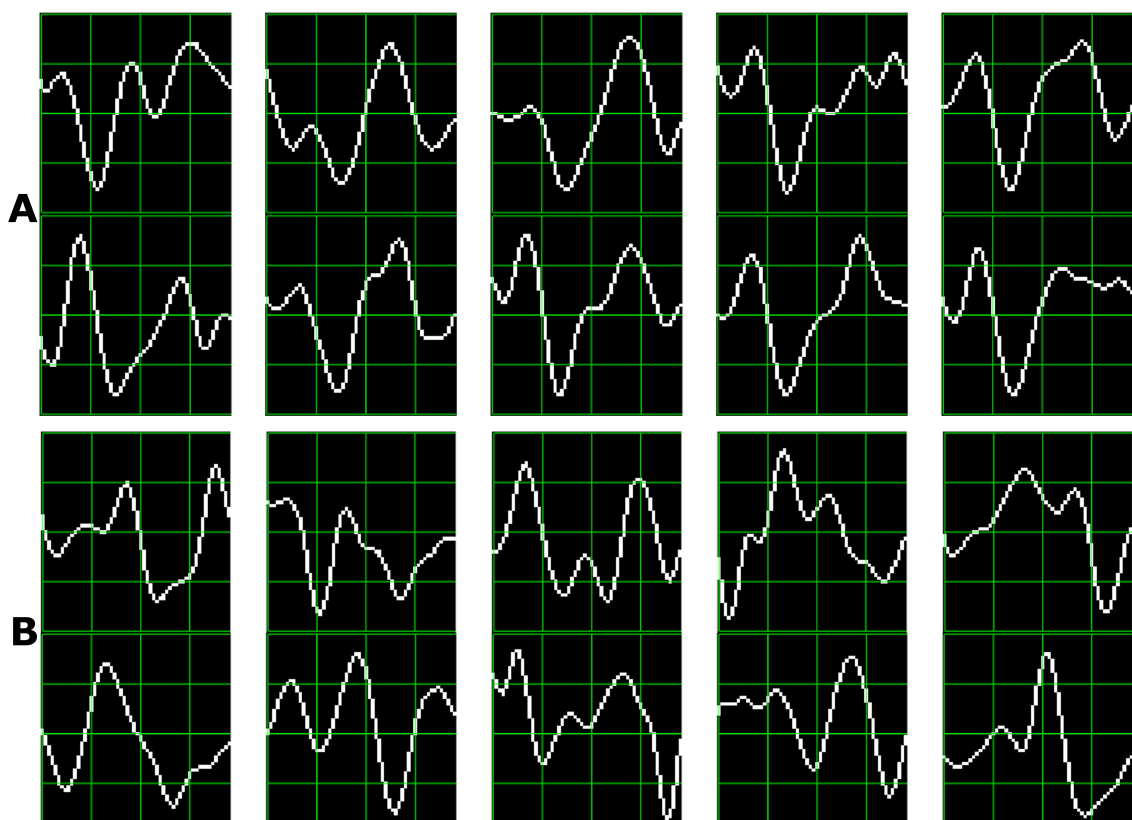


Figure 6. P300 template patches for subjects 8 (A) and 3 (B). Downward deflection is positive polarity.